Letter

Pair Distribution Function from Electron Diffraction in Cryogenic Electron Microscopy: Revealing Glassy Water Structure

João Batista Souza Junior,* Gabriel Ravanhani Schleder, Felippe Mariano Colombari, Marcelo Alexandre de Farias, Jefferson Bettini, Marin van Heel, Rodrigo Villares Portugal, Adalberto Fazzio, and Edson Roberto Leite*

Cite This: *J. Phys. Chem. Lett.* 2020, 11, 1564−1569

Read Online

ACCESS | Metrics & More | Article Recommendations | SI Supporting Information

ABSTRACT: In recent years, cryogenic electron microscopy (Cryo-EM) has revolutionized the structure determination of wet samples and especially that of biological macromolecules. The glassy-water medium in which the molecules are embedded is considered an almost *in vivo* environment for biological samples. The local structure of amorphous ice is known from neutron- and X-ray-diffraction studies, techniques appropriate for much larger volumes than those used in cryo-EM. We here present a first study of the pair-distribution function $g(r)$ of glassy water under cryo-EM conditions using electron diffraction data. We found $g(r)$ to be between that of low-density amorphous ice and that of supercooled water. Under electron exposure, cubic-ice regions were found to nucleate in thicker glassy-water samples. Our work enables to obtain quantitative structural information using $g(r)$ from cryo-EM.
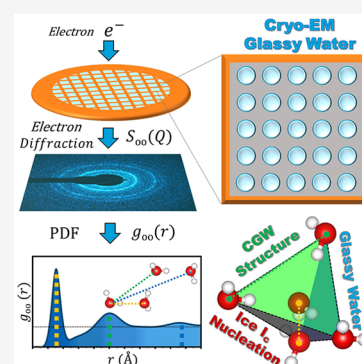
Electron microscopy has in recent years become a fundamental tool for obtaining quantitative structural information from inorganic, organic, and biological materials and compounds.[1,2] An example of this was the development of cryogenic electron microscopy (Cryo-EM), which revolutionized structural biology.[3] In Cryo-EM, a thin film of a solution containing the specimen of interest is frozen rapidly, thus embedding the samples within an amorphous ice matrix or glassy water. The glassy-water film, which provides thermal and mechanical stability to the sample, plays a central role in Cryo-EM data collection.[4] After early research on the biological samples freezing,[5,6] and on the physical properties of glassy water,[7] Dubochet and co-workers[8] carried out a meticulous study optimizing the conditions for routinely obtaining thin films of amorphous ice, free of hexagonal (I_h), or cubic crystalline ice (I_c). This development formed the basis for the current success of Cryo-EM.

Three different forms of amorphous ice can be distinguished: low density amorphous ice (LDA), high-density amorphous ice (HDA), and very-high-density amorphous ice (VHDA).[9] The structure of amorphous ice has previously been studied by neutron- and X-ray diffraction techniques.[10] These techniques allow access to the intra- and intermolecular pair-distribution function (PDF or $g(r)$) of the system, i.e., the probability density of finding an atom from another.[11] For example, X-ray scattering studies revealed that LDA ice structure contains networks of tetracoordinated hydrogen-bonded water molecules, whereas HDA and VHDA show additional interstitial molecules.[12] However, the details of the

amorphous ice structure in cryo-EM, which we call Cryo-EM Glassy Water (CGW), are not yet well understood. A fundamental question still awaiting an answer is what type of amorphous ice CGW is?

Although the analysis of bulk amorphous ice by neutron diffraction and X-ray scattering are well established, they are not suitable for studying CGW structure due to the small volume of cryo-EM samples. Note also that the interaction of the specimen with electrons is stronger than with neutron- and X-ray,[13] implying that electron diffraction (ED) using transmission electron microscopy (TEM) will yield more PDF information from small cryo-EM volumes. Here, we have developed the pair distribution function from electron diffraction (ePDF) analysis to elucidate the CGW local molecular structure for typical cryo-EM volumes (Figure S1 in the Supporting Information). The ePDF is a powerful tool for analyzing nanomaterials,[14] and here, we are applying this technique for the study of frozen liquids. From the ED patterns, we obtained the real-space interatomic distance correlation function using the eRDF software,[15] which was modified to obtain the molecular $g_{OO}(r)$. Details of the procedure used to obtain the $g_{OO}(r)$ from ED pattern can be found in the Supporting Information (see Figures S2−S8).

The $g_{OO}(r)$ provides information on intermolecular distances; here, the O−O distances among water molecules,[16] and the information about the O−H distances can be found in Figure S6. A detailed analysis of the PDF patterns obtained requires their comparison with reference patterns. The reference material we used includes molecular dynamics simulations (MD), static simulations, and standard experimental XRD scattering results from the literature. The $g_{OO}(r)$ values of liquid water, supercooled water, and amorphous LDA were obtained from MD calculations; we simulated I_c and I_h crystalline ice $g_{OO}(r)$ using CIF files (static simulations); and $g_{OO}(r)$ values from XRD scattering for liquid water,[16] supercooled water,[17] and LDA[12] were obtained from the literature. Figure 1 shows the experimental ePDF for CGW
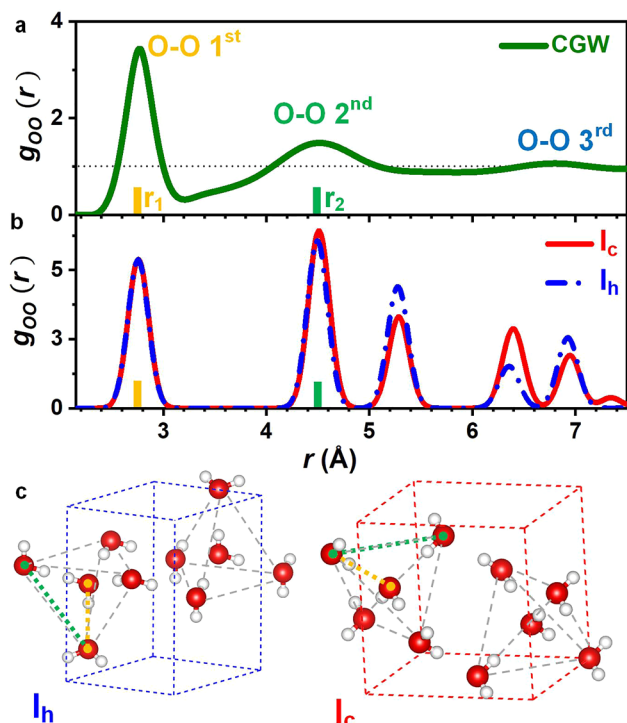
Figure 1. (a) ePDF $g_{OO}(r)$ for a CGW film. (b) Simulated O−O PDF $g_{OO}(r)$ (r) for both hexagonal (I_h) and cubic (I_c) bulk crystalline ice showing the first two comparable neighboring O−O distances (r colored vectors) that can be visualized in both (c), I_c and I_h unit cells.

compared to static simulations, and Figure 2 shows the MD analysis and literature data. Note that the CGW $g_{OO}(r)$ pattern, Figure 1, shows a series of broad peaks, reflecting a specific molecular coordination shell related to the organization of the H_2O molecules in the glassy state, being the O−O distances indexed based on the simulated and literature $g_{OO}(r)$ (see Figure S6 in the Supporting Information).

Figure 1a shows the ePDF $g_{OO}(r)$ for a typical thin CGW film. All samples' $g_{OO}(r)$ indicate that no ordering beyond 8 Å is observed for CGW.[18] Simulations of PDF $g_{OO}(r)$ for I_h and I_c bulk phases are similar for the first neighbors, as shown in Figure 1b and visualized in their respective unit cells, Figure 1c, which also displays the similarity in the distances of the first neighbors (r vectors) inside the water tetrahedron displayed within their unit cells (see Figure S9). Although it is not possible to differentiate the local structure between the CGW and both crystal structures, the first two coordination shells (O−O molecular distances) observed for CGW in Figure 1a
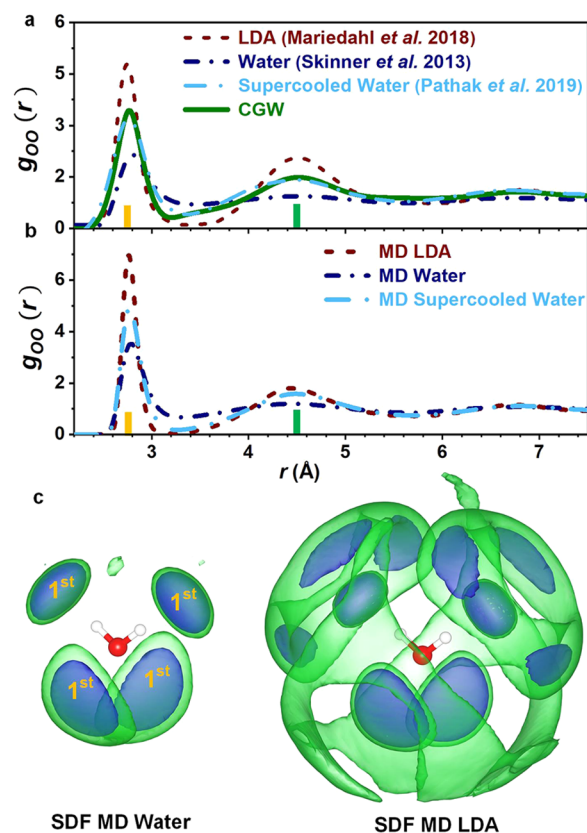
Figure 2. (a) PDF $g_{OO}(r)$ of low-density amorphous ice (LDA, obtained from very-high-density amorphous ice annealed at 140 K) from Mariedahl et al.,[12] liquid water (ambient temperature) from Skinner et al.,[16] and supercooled water (235 K) from Pathak et al.[17] obtained by X-ray analysis, compared to ePDF $g_{OO}(r)$ of a typical CGW thin film (frozen at 90 K and stored at 77 K). (b) $g_{OO}(r)$ obtained by molecular dynamics of LDA (77 K), liquid water (298 K), and supercooled water (233 K). (c) Spatial distribution function (SDF) of the water (left) and LDA (right) obtained by molecular dynamics. Two isosurfaces are shown: 55 (green) and 95 (blue) molecules nm^{-3}; larger isosurface values indicate a larger spatial concentration of molecules.

clearly are correlated with the lengths of r vectors shown in Figure 1b,c. On the basis of this model, the $g_{OO}(r)$ peaks in Figure 1a were indexed as follows, the first peak $g_1(r)$ is related to the local structure in the first coordination shell located at r_1 (O−O 1st, yellow line, 2.77 Å), which is directly correlated with the tetrahedrality of the water generated by its hydrogen bonds (two intermolecular H−O and two O−H through the lone pairs), Figure S10. The ePDF $g_{OO}(r)$ displayed in Figure 1a also presents two other peaks (coordination shells), demonstrating that the local structure of CGW maintains at least three structured neighbor shells. The second O−O peak $g_2(r)$ is associated with the O−O distance from the edge length of the water tetrahedron (O−O 2nd, green line, 4.5 Å) and the third O−O peak $g_3(r)$ is a convolution of the two peaks at 6.3 and 6.9 Å found in both I_h and I_c phases. However, it is clear that the CGW O−O arrangement does not have similarity with a solid crystalline structure, displaying a typical $g(r)$ feature of amorphous samples. Next, a CGW analysis is presented in Figure 2 with the MD and literature data for amorphous ice structures.

The structure of the CGW is compared to that given by Skinner et al.[16] for liquid water, by Pathak et al.[17] for
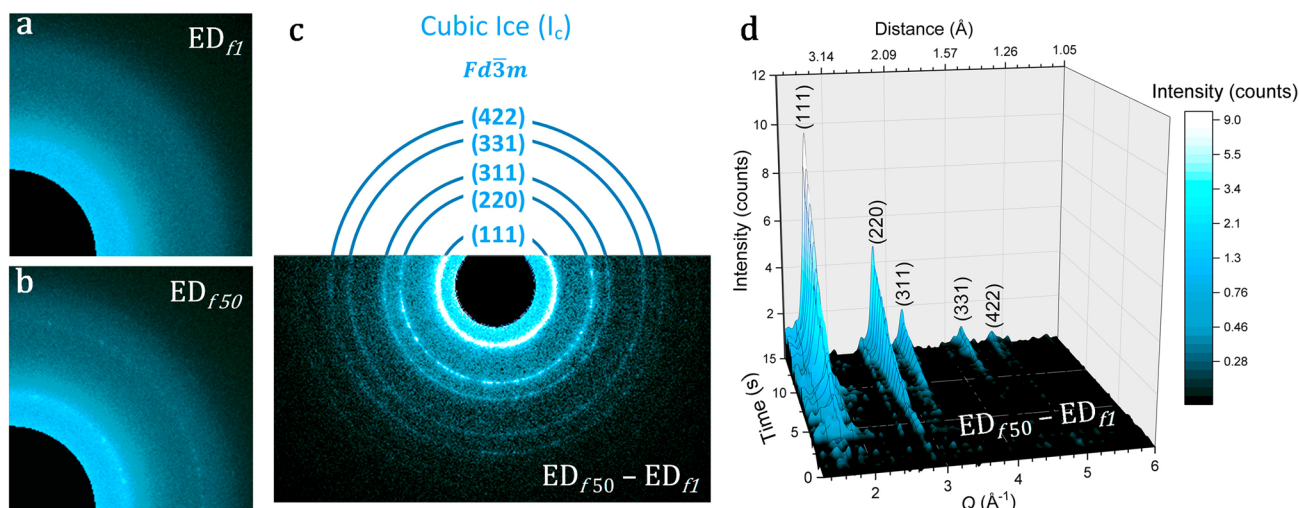
Figure 3. ED-TEM results for a 500 nm thick CGW film showing the (a) electron diffraction (ED) for frame 1 (ED_{f_1}) and (b) frame 50 (ED_{f50}). (c) Difference between images ($ED_{f_{50}}$) and (ED_{f_1}) used to highlight the diffraction spots from the nucleated crystalline ice that were indexed to cubic phase I_c. (d) Time evolution graphic showing the diffraction intensity profile for crystalline ice only (amorphous background subtracted, ($ED_{f_{50}}$) − (ED_{f_1})).

supercooled water, and by Mariedahl et al.[12] for LDA $g_{OO}(r)$ (Figure 2a). The local tetrahedral structure in $g_1(r)$ shows a coordination number n_{OO} of 4.0 (from 2.2 to 3.4 Å), which is similar to that for the supercooled water from MD (see Figure S8) but still lower than those observed experimentally for supercooled water (4.39) and LDA samples (4.3). Although the first peak position r_1 (2.77 Å) is similar to those for CGW, supercooled water (≈2.8 Å), and LDA phases (2.75 Å), the peak height for CGW (3.45) is closer to that of supercooled water reported by Pathak et al. (3.19)[17] and smaller than that for the LDA phase (4.79) obtained by Mariedahl et al.[12] The ePDF $g_{OO}(r)$ displayed in Figure 2a also presents two other peaks (coordination shells), demonstrating that the local structure of CGW maintains at least three structured neighbor shells.

The molecular network of liquid water is proposed to be a dynamic mixture of a coexisting low-density liquid (LDL) and a high-density liquid (HDL).[19,20] Upon cooling, each has its corresponding amorphous form, a LDA and a HDA. Their structural difference relies on the hydrogen bond assembly between two neighboring tetrahedral structures (illustrated in Figure S11). While the former presents a hydrogen bonding pattern between two tetrahedra, involving two water molecules of both structures, the latter presents a disruption of such interactions since higher pressures impose a closer contact. In the liquid state, hydrogen bonding between tetrahedral nearest neighbors is dynamically changing by keeping (LDL) or losing (HDL) this structure. Such interchange briefly brings water molecules to excluded (depleted) regions (the region between the two first peaks $g_1(r)$ and $g_2(r)$, 3.0 Å < r < 4.2 Å).[21−23]

MD simulations of LDA ice, supercooled water, and liquid water were performed to clarify the CGW $g_{OO}(r)$ findings. In Figure 2b the $g_{OO}(r)$ simulated from MD for LDA, liquid, and supercooled water are compared. For the supercooled state, the liquid water tetrahedrality is increased, giving peaks that are more well-defined toward the LDA pattern.[17] This situation is elucidated by the spatial distribution function (SDF) in Figure 2c, showing that the LDA presents a more ordered tetrahedral network structure beyond first neighbors,

while liquid water presents orientational deviations and also correlations in the depletion region, related to its dynamical behavior (Figure S12).[23] Our results suggest that the CGW structure has an intermediate ordering between two continuous thermodynamic metastable states:[21] the supercooled liquid water and the LDA structures, based on the intensities of the first two $g_{OO}(r)$ peaks (see Figure 2a). The ordering is smaller than supercooled water (Figure 2b) near its Widom line of liquid−liquid (HDL/LDL) transition at 229.2 K.[20] Therefore, under cryo-EM conditions, the samples should have solidified in the 240−250 K temperature range, before reaching deep supercooled temperatures which display increased LDL tetrahedrality.[17]

CGW structure formation is related to its 2D morphology and preparation cooling rate. Compared to hyperquenched glassy water (HGW) that is frozen from micrometer-sized water droplets,[24] the thin CGW nanomembrane (<500 nm) reaches temperatures below the T_g much faster than HGW. The cooling rate is inversely proportional to the square of the thickness (freezing front penetration from the surface to the center of the sample).[25] Therefore, the cooling rate at the center of the water sample increases with smaller sizes (see Figure S13). It is known that the fraction of LDL increases by lowering the temperature.[17,19] As the morphology of HGW water samples is bigger, they take longer time to reach the T_g, increasing the supercooling before solidifying and leading to an increased LDA (solidified from the parent LDL) character. Differently, it is expected that the CGW have a higher amount of HDL phase as its faster cooling rate generates an amorphous ice with structure between liquid water and LDA, analogue to a supercooled water. Note that both CGW and HGW do not cross the T_c avoiding crystal formation, thus keeping the amorphous structure. Therefore, one can argue that CGW is frozen maintaining a higher fraction of HDL whereas HGW takes longer to become solid, having enough time to increase the LDL content. Having established that CGW is a frozen metastable structure, if annealed, it would have a transition above the T_g to the kinetically stable LDA.

In addition to ePDF analysis, ED-TEM can also be used to evaluate CGW stability. Here, ice crystallization induced by the electron beam was investigated using a series of ED with a dose rate of 12 $e^- Å^{-2}$ s and 3.33 frames s^{-1} (3.6 $e^- Å^{-2}$ total dose by frame). A time-dependent crystallization pattern was recorded, as shown in Figure 3. The first ED pattern after 0.3 s of exposure (ED_{f_1}) for a CGW film with thickness of 500 nm clearly shows an amorphous scattering profile with the absence of diffraction spots, Figure 3a. In contrast, Figure 3b shows the final pattern $ED_{f_{50}}$ after 15 s of exposure (frame 50, total dose of 180 $e^- Å^{-2}$) displaying diffraction spots along with the amorphous profile, i.e., the formation of crystalline ice within the amorphous network. By subtracting the ED_{f_1} image from the $ED_{f_{50}}$ one, the amorphous scattering content can qualitatively be subtracted from the final ED, to thus reveal the diffraction rings of the emerging crystalline phase. Figure 3c shows five diffraction rings that are well indexed for the I_c phase. To clarify, Figure 3d shows a qualitative time-dependent crystallization profile. $I(Q)$ at 1.70 $Å^{-1}$ (d = 3.69 Å), which corresponds to the first and most intense diffraction ring in the $ED_{f_{50}}$, clearly displays an intensity raise with time due to the electron exposure. This process begins around 5 s, accumulating a total dose of 60 $e^- Å^{-2}$. A second peak occurs at 2.78 $Å^{-1}$ (2.26 Å), and the other three peaks of lower intensities can be only detected in the last frames. Although I_c peaks are seen in the final $ED_{f_{50}}$ compared to ED_{f_1}, the amorphous content is still the majority phase.

The results indicate that the transition from CGW to crystalline ice under electron exposure occurs via the I_c phase and not via the thermodynamically stable[26] I_h phase. The pure amorphous ice film is a metastable material that nucleates crystalline ice when energy is added to the system such as increasing the temperature or, in the cryo-EM case, by the incidence of high-energy electrons.[27] As discussed by Debenedetti and coauthors,[9] metastable amorphous ice has a transition to LDA structure when annealed above the T_g (136 K), and at 150 K I_c nucleation begins. Samples were prepared in liquid ethane at 90 K and ambient pressure and were kept at 77 K (liquid N_2 bath) prior to the TEM experiments, which were conducted at a vacuum <10^{-7} Pa and a temperature of approximately 77 K using the N_2-reservoir cryo-holder. Therefore, since the I_c nucleation temperature was never surpassed, we assume that the crystallization only occurs due to electron-beam inelastic-scattering interactions.

Crystallization of ice within cryo-EM samples induced by the electron beam is a thickness-dependent phenomenon. Whereas the thickest sample (500 nm) showed I_c nucleation, no diffraction spots were observed for the thinnest sample (90 nm) under otherwise identical acquisition conditions (Figure S14). Correspondingly, the intermediate-thickness sample (310 nm) showed an intermediate amount of crystallization. The thickness-dependent behavior increases with the electron interaction volume, and thus with the probability of an inelastic scattering. The inelastic mean free path of electrons in CGW films at 120 kV was previously measured to be between 160 and 230 nm.[28,29] Considering these values as lower limits at 200 kV, it is expected that the 90 nm film will allow almost no inelastic-scattering interaction, thus no crystallization. Furthermore, the inelastic mean free path of electrons in liquid water was reported to be 290 nm at 200 kV,[30] which is also consistent with our observations of crystallization on the 310

nm film. By using ePDF, apart from the I_c nucleation, no significant differences on $g_{OO}(r)$ were observed for CGW samples with different thickness (Figures S15 and S16). This thickness-dependent behavior observed is highly relevant for microscopists planning their cryo-EM experiments avoiding *in situ* ice crystallization.

In summary, we have shown that ePDF is a powerful tool for studying frozen liquids in the amorphous state. Given the central role that water plays in life as we know it, our methodology may add significantly to the understanding of this precious material. CGW structure can be readily investigated reinforcing the importance of thickness and cooling rates applied in cryo-EM sample preparation.[31] As a dynamic mixture of LDL water and HDL water, cryo-EM vitreous water possesses more high-density structures than LDA vitreous water, yet fewer than liquid water. Our results open new opportunities to study vitreous water structure and its interaction with solutes, nanoparticles, and biological samples, as well as the vitreous state of different organic and inorganic solvents and solutions.

■ ASSOCIATED CONTENT

ⓢ Supporting Information

The Supporting Information is available free of charge at https://pubs.acs.org/doi/10.1021/acs.jpclett.0c00171.

Experimental section and computational details; scheme of Cryo-EM TEM grid; SAED pattern of gold for reciprocal space calibration; $I(Q)$, $S(Q)_{mol}$, $S_{OO}(Q)$, $G(r)_{mol}$, $G_{OO}(r)$, and n_{OO} for the CGW sample; simulated O−O PDF g_{OO}, schematic representation of molecular interactions forming water tetrahedron for HDA and LDA; spatial distribution function (SDF) difference between liquid water and LDA; hypothetical time−temperature diagram for water cooling; ED and TEM images, SAED patterns, $I(Q)$, $S_{OO}(Q)$, and $g_{OO}(r)$ for CGW with different thicknesses (PDF)

■ AUTHOR INFORMATION

Corresponding Authors

João Batista Souza Junior − *Brazilian Nanotechnology National Laboratory (LNNano), Brazilian Center for Research in Energy and Materials (CNPEM), 13083-970 Campinas, Brazil;* ⓞ orcid.org/0000-0002-1725-3552; Email: joao.junior@lnnano.cnpem.br

Edson Roberto Leite − *Brazilian Nanotechnology National Laboratory (LNNano), Brazilian Center for Research in Energy and Materials (CNPEM), 13083-970 Campinas, Brazil; Department of Chemistry, Federal University of São Carlos, 13565-905 São Carlos, SP, Brazil;* Email: edson.leite@lnnano.cnpem.br

Authors

Gabriel Ravanhani Schleder − *Brazilian Nanotechnology National Laboratory (LNNano), Brazilian Center for Research in Energy and Materials (CNPEM), 13083-970 Campinas, Brazil; Federal University of ABC (UFABC), 09210-580 Santo André, São Paulo, Brazil;* ⓞ orcid.org/0000-0003-3129-8682

Felippe Mariano Colombari − *Brazilian Nanotechnology National Laboratory (LNNano), Brazilian Center for Research in Energy and Materials (CNPEM), 13083-970 Campinas, Brazil;* ⓞ orcid.org/0000-0002-5431-1301

Marcelo Alexandre de Farias − *Brazilian Nanotechnology National Laboratory (LNNano), Brazilian Center for Research in Energy and Materials (CNPEM), 13083-970 Campinas, Brazil*

Jefferson Bettini − *Brazilian Nanotechnology National Laboratory (LNNano), Brazilian Center for Research in Energy and Materials (CNPEM), 13083-970 Campinas, Brazil*

Marin van Heel − *Brazilian Nanotechnology National Laboratory (LNNano), Brazilian Center for Research in Energy and Materials (CNPEM), 13083-970 Campinas, Brazil; Netherlands Centre for Electron Nanoscopy (NeCEN),, 2333 CC Leiden, The Netherlands; Faculty of Natural Sciences, Imperial College London, London SW7 2AZ, U.K.*

Rodrigo Villares Portugal − *Brazilian Nanotechnology National Laboratory (LNNano), Brazilian Center for Research in Energy and Materials (CNPEM), 13083-970 Campinas, Brazil;* orcid.org/0000-0003-0463-8717

Adalberto Fazzio − *Brazilian Nanotechnology National Laboratory (LNNano), Brazilian Center for Research in Energy and Materials (CNPEM), 13083-970 Campinas, Brazil; Federal University of ABC (UFABC), 09210-580 Santo André, São Paulo, Brazil;* orcid.org/0000-0001-5384-7676

Complete contact information is available at:
https://pubs.acs.org/10.1021/acs.jpclett.0c00171

Notes

The authors declare no competing financial interest.

■ REFERENCES

(1) Jones, C. G.; Martynowycz, M. W.; Hattne, J.; Fulton, T. J.; Stoltz, B. M.; Rodriguez, J. A.; Nelson, H. M.; Gonen, T. The CryoEM Method MicroED as a Powerful Tool for Small Molecule Structure Determination. *ACS Cent. Sci.* **2018**, *4*, 1587−1592.

(2) Brázda, P.; Palatinus, L.; Babor, M. Electron Diffraction Determines Molecular Absolute Configuration in a Pharmaceutical Nanocrystal. *Science* **2019**, *364*, 667−669.

(3) Glaeser, R. M.; Han, B.-G.; Csencsits, R.; Killilea, A.; Pulk, A.; Cate, J. H. Factors that Influence the Formation and Stability of Thin, Cryo-EM Specimens. *Biophys. J.* **2016**, *110*, 749−755.

(4) Adrian, M.; Dubochet, J.; Lepault, J.; Mc-Dowall, A. W. Cryoelectron Microscopy of Viruses. *Nature* **1984**, *308*, 32−36.

(5) Fernández-Morán, H. Low-Temperature Preparation Techniques for Electron Microscopy of Biological Specimens Based on Rapid Freezing with Liquid Helium II. *Ann. N. Y. Acad. Sci.* **1960**, *85*, 689−713.

(6) Taylor, K. A. Structure Determination of Frozen, Hydrated, Crystalline Biological Specimens. *J. Microsc.* **1978**, *112*, 115−125.

(7) Brüggeller, P.; Mayer, E. Complete Vitrification in Pure Liquid Water and Dilute Aqueous Solutions. *Nature* **1980**, *288*, 569−571.

(8) Dubochet, J.; Chang, J. J.; Freeman, R.; Lepault, J.; McDowall, A. W. Frozen Aqueous Suspensions. *Ultramicroscopy* **1982**, *10*, 55−61.

(9) Debenedetti, P. G.; Stanley, H. E. Supercooled and Glassy Water. *Phys. Today* **2003**, *56*, 40−46.

(10) Amann-Winkel, K.; Böhmer, R.; Fujara, F.; Gainaru, C.; Geil, B.; Loerting, T. Colloquium: Water's Controversial Glass Transitions. *Rev. Mod. Phys.* **2016**, *88*, 011002.

(11) Tran, D. T.; Svensson, G.; Tai, C.-W. SUePDF: A Program to Obtain Quantitative Pair Distribution Functions from Electron Diffraction Data. *J. Appl. Crystallogr.* **2017**, *50*, 304−312.

(12) Mariedahl, D.; Perakis, F.; Späh, A.; Pathak, H.; Kim, K. H.; Camisasca, G.; Schlesinger, D.; Benmore, C.; Pettersson, L. G. M.; Nilsson, A.; et al. Xray Scattering and O-O Pair-Distribution Functions of Amorphous Ices. *J. Phys. Chem. B* **2018**, *122*, 7616−7624.

(13) Henderson, R. The Potential and Limitations of Neutrons, Electrons and XRays for Atomic Resolution Microscopy of Unstained Biological Molecules. *Q. Rev. Biophys.* **1995**, *28*, 171−193.

(14) Schleder, G. R.; Azevedo, G. M.; Nogueira, I. C.; Rebelo, Q. H.; Bettini, J.; Fazzio, A.; Leite, E. R. Decreasing Nanocrystal Structural Disorder by Ligand Exchange: An Experimental and Theoretical Analysis. *J. Phys. Chem. Lett.* **2019**, *10*, 1471−1476.

(15) Shanmugam, J.; Borisenko, K. B.; Chou, Y. J.; Kirkland, A. I. eRDF Analyser: An Interactive GUI for Electron Reduced Density Function Analysis. *SoftwareX* **2017**, *6*, 185−192.

(16) Skinner, L. B.; Huang, C.; Schlesinger, D.; Pettersson, L. G.; Nilsson, A.; Benmore, C. J. Benchmark Oxygen-Oxygen Pair-Distribution Function of Ambient Water from X-Ray Diffraction Measurements with a Wide Q-Range. *J. Chem. Phys.* **2013**, *138*, 074506.

(17) Pathak, H.; Späh, A.; Kim, K. H.; Tsironi, I.; Mariedahl, D.; Blanco, M.; Huotari, S.; Honkimäki, V.; Nilsson, A. Intermediate Range O−O Correlations in Supercooled Water Down to 235 K. *J. Chem. Phys.* **2019**, *150*, 224506.

(18) Dubochet, J.; Lepault, J.; Freeman, R.; Berriman, J. A.; Homo, J. C. Electron Microscopy of Frozen Water and Aqueous Solutions. *J. Microsc.* **1982**, *128*, 219−237.

(19) Poole, P. H.; Sciortino, F.; Essmann, U.; Stanley, H. E. Phase Behaviour of Metastable Water. *Nature* **1992**, *360*, 324−328.

(20) Kim, K. H.; Späh, A.; Pathak, H.; Perakis, F.; Mariedahl, D.; AmannWinkel, K.; Sellberg, J. A.; Lee, J. H.; Kim, S.; Park, J.; et al. Maxima in the Thermodynamic Response and Correlation Functions of Deeply Supercooled Water. *Science* **2017**, *358*, 1589−1593.

(21) Stanley, H. E.; Mishima, O. The Relationship Between Liquid, Supercooled and Glassy Water. *Nature* **1998**, *396*, 329−335.

(22) Gallo, P.; Stanley, H. E. Supercooled Water Reveals its Secrets. *Science* **2017**, *358*, 1543−1544.

(23) Svishchev, I. M.; Kusalik, P. G. Structure in Liquid Water: A Study of Spatial Distribution Functions. *J. Chem. Phys.* **1993**, *99*, 3049−3058.

(24) Johari, A. M. E.; Hallbrucker, G. P. The Glass−Liquid Transition of Hyperquenched Water. *Nature* **1987**, *330*, 552.

(25) Kohl, I.; Bachmann, L.; Mayer, E.; Hallbrucker, A.; Loerting, T. Glass Transition in Hyperquenched Water? *Nature* **2005**, *435*, E1−E2.

(26) Hudait, A.; Molinero, V. What Determines the Ice Polymorph in Clouds? *J. Am. Chem. Soc.* **2016**, *138*, 8958−8967.

(27) Gallo, P.; Amann-Winkel, K.; Angell, C. A.; Anisimov, M. A.; Caupin, F.; Chakravarty, C.; Lascaris, E.; Loerting, T.; Panagiotopoulos, A. Z.; Russo, J.; et al. Water: A Tale of Two Liquids. *Chem. Rev.* **2016**, *116*, 7463−7500.

(28) Baumeister, W. Electron Tomography of Molecules and Cells. *Trends Cell Biol.* **1999**, *9*, 81−85.

(29) Feja, B.; Aebi, U. Determination of the Inelastic Mean Free Path of Electrons in Vitrified Ice Layers for On-Line Thickness Measurements by Zero-Loss Imaging. *J. Microsc.* **1999**, *193*, 15−19.

(30) Nguyen-Truong, H. T. Low-Energy Electron Inelastic Mean Free Paths for Liquid Water. *J. Phys.: Condens. Matter* **2018**, *30*, 155101.

(31) Giovambattista, N.; Starr, F. W.; Poole, P. H. Influence of Sample Preparation on the Transformation of LowDensity to High-

Density Amorphous Ice: An Explanation Based on the Potential Energy Landscape. *J. Chem. Phys.* **2017**, *147*, 044501.